

# Oscillation Waveforms and Amplitudes from Hot Spots on Neutron Stars

Nevin Weinberg

Department of Astronomy and Astrophysics, University of Chicago  
5640 South Ellis Avenue, Chicago, IL 60637  
nweinber@midway.uchicago.edu

M. Coleman Miller

Department of Astronomy, University of Maryland  
College Park, MD 20742-2421  
miller@astro.umd.edu

Donald Q. Lamb

Department of Astronomy and Astrophysics and Enrico Fermi Institute  
University of Chicago, 5640 South Ellis Avenue, Chicago, IL 60637  
lamb@pion.uchicago.edu

## ABSTRACT

The discovery of high-amplitude brightness oscillations during type I X-ray bursts from six low-mass X-ray binaries has provided a powerful new tool to study the properties of matter at supranuclear densities, the effects of strong gravity, and the propagation of thermonuclear burning. There is substantial evidence that these brightness oscillations are produced by spin modulation of one or two localized hot spots confined to the stellar surface. It is therefore important to calculate the expected light curves produced by such hot spots under various physical assumptions, so that comparison with the observed light curves may most sensitively yield information about the underlying physical quantities. In this paper we make general relativistic calculations of the light curves and oscillation amplitudes produced by a rotating neutron star with one or two hot spots as a function of spot size, stellar compactness, rotational velocity at the stellar surface, spot location, orientation of the line of sight of the observer, and the angular dependence of the surface specific intensity. For the case of two emitting spots we also investigate the effects of having spot separations less than  $180^\circ$  and the effects of having asymmetries in the brightness of the two spots. We find that stellar rotation and beaming of the emission tend to increase the observed oscillation amplitudes whereas greater compactness and larger spot size tend to decrease them. We also show that when two emitting spots are either non-antipodal or asymmetric in brightness, significant power at the first harmonic is generated. By applying these results to 4U 1636–536, whose two emitting spots produce power at the first harmonic, we place strong constraints on the neutron star’s magnetic field geometry. We also show that the data on the phase lags between photons of different

energies in the persistent pulsations in SAX J1808–58 can be fit well with a model in which the observed hard leads are due to Doppler beaming.

*Subject headings:* stars: neutron — equation of state — gravitation — relativity — X-rays: bursts

## 1. INTRODUCTION

The study of neutron stars is attractive in part because of the fundamental issues of physics that can be addressed. These include the behavior of spacetime in strong gravity, the equation of state of matter at supranuclear densities, and the propagation of thermonuclear burning in degenerate matter, an issue which has relevance to many astrophysical events including classical novae and Type Ia supernovae.

The discovery with the *Rossi X-ray Timing Explorer (RXTE)* of highly coherent brightness oscillations during type I (thermonuclear) X-ray bursts from six low mass X-ray binaries (LMXB) (for reviews see, e.g., Strohmayer, Zhang & Swank 1997b; Smith, Morgan & Bradt 1997; Zhang et al. 1996; and Strohmayer et al. 1997c) has provided a potentially sensitive new tool to understand these fundamental issues. The burst oscillations are thought to be produced by spin modulation of one or two localized thermonuclear hot spots that are brighter than the surrounding surface. The existence of the oscillations, as well as some of the reported behavior of their amplitudes (see, e.g., Strohmayer et al. 1997b) seems to confirm the pre-existing theoretical expectation that X-ray bursts on neutron stars are caused by ignition at a point followed by thermonuclear propagation around the surface (e.g., Fryxell & Woosley 1982; Nozakura et al. 1984; Bildsten 1995). The observed waveforms of these oscillations, and their dependence on time and photon energy, can in principle be used to constrain the mass and radius of the star and the velocity and type of thermonuclear propagation. Such information can only be extracted by detailed comparison of theoretical waveforms with the data.

Here we conduct the most complete existing survey of the properties of the light curves and resultant oscillation amplitudes for one or two expanding hot spots. We calculate light curves and oscillation amplitudes as a function of stellar compactness, rotational velocity at the stellar surface, spot size and location, orientation of the line of sight, angular dependence of the specific intensity, and spot asymmetries. Our calculations follow a procedure similar to that of Pechenick, Ftaclas, & Cohen (1983), Strohmayer (1992), and Miller & Lamb (1998), but our survey is more comprehensive than these previous treatments in that we fully investigate the effects of an expanding spot size on the light curves and oscillation amplitudes, while also exploring the effects of gravity, stellar rotation, viewing geometries, and anisotropic emission. In addition, we present the first calculations of the effects of having two non-antipodal spots as well as the effects of asymmetries in spot brightness.

In § 2 we describe our assumptions and the calculational method. In § 3 we present our results. We show that for small spot sizes the oscillation amplitude has only a weak dependence on spot size, but that as the spot grows the dependence becomes very strong. We also show that stellar rotation, beaming functions and spot asymmetries all tend to increase the observed oscillation amplitudes whereas greater compactness and larger spot sizes tend to decrease the amplitudes. In § 4 we exhibit applications of these results to data on the amplitudes of two harmonics in 4U 1636–536 and on the phase lags versus energy for SAX J1808–3658. We discuss our results and present our conclusions in § 5.

## 2. CALCULATIONAL METHOD

We make the following assumptions in our calculations:

1. *The observed radiation comes from one or two emitting spots on the surface.* The sources with strong bursts tend to have persistent accretion rates a factor of  $\sim 10$ – $100$  less than the Eddington critical luminosity  $L_E$  at which the radial radiation force balances gravity, whereas the peak luminosity of the bursts is typically close to  $L_E$ . The flux from the burning regions therefore greatly exceeds the flux from the quiescent regions, so for much of the burst this is a plausible approximation.
2. *The radiation is homogeneous and emitted isotropically unless noted otherwise.* This assumption is made for simplicity, as presently there is no physical evidence that suggests whether or not the photon emission from the hot spots is isotropic and homogeneous.
3. *If there are two spots, they are identical and both grow at the same velocity unless noted otherwise.* This assumption is also made for simplicity. Although the geometry of the two magnetic poles is unlikely to be identical, not enough is known about their structure to realistically model non-identical spots.
4. *The exterior spacetime of the neutron star is the Schwarzschild spacetime.* We neglect the effect of frame dragging due to stellar rotation because it only generates small second order effects for the rotation rates of interest (see Lamb & Miller 1995 and Miller & Lamb 1996).

We compute the waveform of the oscillation as seen at infinity using the procedure of Pechenick et al. (1983). Figure 1 shows our coordinate system and angle definitions. The photons emitted from the star travel along null geodesics which, for a Schwarzschild geometry, satisfy the equation (Misner, Thorne, and Wheeler 1973, p. 673)

$$\left(\frac{1}{r^2} \frac{dr}{d\phi}\right)^2 + \left(\frac{1 - 2M/r}{r^2}\right) = \frac{1}{b^2} \quad (1)$$

where  $r$  and  $\phi$  are spherical coordinates,  $M$  is the gravitational mass of the star, and  $b$  is the impact parameter of the photon orbit. In both the above equation and throughout, we use

geometrized units in which  $G = c \equiv 1$ . If the photon is initially at a global azimuthal angle  $\phi = 0$ , then the global azimuthal angle at infinity follows from equation (1) and is (Pechenick et al. 1983, eq. [2.12])

$$\phi_{\text{obs}} = \int_0^{M/R} \left[ u_b^2 - (1 - 2u) u^2 \right]^{-1/2} du \quad (2)$$

where  $u_b = M/b$ . Note that not all of this angle is due to light deflection: for example, a photon emitted tangent to the radial vector in flat spacetime will have an angle  $\phi_{\text{obs}} = \pi/2$  at infinity. The maximum angle occurs when  $b = b_{\text{max}} = R(1 - 2M/R)^{-1/2}$  and is given by (Pechenick et al. 1983, eq. [2.13])

$$\phi_{\text{max}} = \int_0^{M/R} \left[ \left( 1 - \frac{2M}{R} \right) \left( \frac{M}{R} \right)^2 - (1 - 2u) u^2 \right]^{-1/2} du \quad (3)$$

The observer at infinity cannot see the spot if the observer’s azimuthal angle exceeds  $\phi_{\text{max}}$ .

For each phase of rotation we compute the projected area of many small elements of a given finite size spot. We then build up the light curve of the entire spot by superposing the light curve of all the small elements. We chose a grid resolution such that the effect of having a finite number of small elements produces a fractional error  $< 10^{-4}$  in the computed oscillation amplitudes. For isotropic emission the intensity of radiation at a given rotational phase as seen by an observer at infinity is directly proportional to the projected area of the spot. To investigate the effect of anisotropic emission we include a flux distribution function in the intensity,  $f(\delta)$ , where  $\delta$  is the angle between the surface normal and the photon propagation direction. The intensity is then proportional to the product of the projected area of the spot (which is proportional to  $\cos \delta$ ) and  $f(\delta)$ . We consider two types of anisotropic emission: cosine (“pencil”) beaming, in which  $f(\delta) = \cos \delta$ , and sine (“fan”) beaming, in which  $f(\delta) = \sin \delta$ .

The intensity distribution of an emitting spot is aberrated by the rotation of the star, and the photon frequency is Doppler shifted by the factor  $1/[\gamma(1 - v \cos \zeta)]$ . Here  $v$  is the velocity at the stellar equator,  $\gamma = (1 - v^2)^{-1/2}$ , and  $\zeta$  is the angle between the direction of photon propagation and the local direction of rotation. The inferred spin frequencies of these neutron stars are  $\sim 300$  Hz, implying surface velocities  $v \sim 0.1c$  for stellar radii  $R \sim 10$  km.

After computing the oscillation waveform using the above approach, we Fourier-analyze the resulting light curve to determine the oscillation amplitudes and phases as a function of photon energy at different harmonics.

### 3. RESULTS

As discussed in the introduction, the basic quantities of interest include the mass and radius of the neutron stars in bursting sources and the nature and speed of thermonuclear propagation on the stellar surface. We therefore need to relate these fundamental quantities to the observables, such as the oscillation waveform as a function of time and photon energy. We do this by computing

theoretical waveforms using different assumptions about the compactness of the star, the angular size of the burning region, the angular location of the observer and magnetic pole relative to the stellar rotation axis, the surface rotation velocity of the star, and the angular distribution of the specific intensity at the surface. In this section we consider each of these effects separately, to isolate the effect they have on the waveform and facilitate interpretation of the data. Here we always quote the fractional rms amplitude of brightness oscillations. We also quote only bolometric amplitudes in this section; as shown by Miller & Lamb (1998), oscillations in the energy spectrum of the source may yield substantially higher amplitudes in the countrate spectrum measured by bandpass-limited instruments such as *RXTE*.

### 3.1. Waveforms

The decrease in oscillation amplitude as the bursts in some sources progress (Strohmayer et al. 1997b) may suggest an initially localized emission spot that expands via relatively slow ( $\sim 10^6 \text{ cm s}^{-1}$ ) thermonuclear propagation. If so, we would expect that the waveforms from burst oscillations would reflect a variety of spot sizes. We therefore consider spots that range from pointlike to those with an angular radius of  $180^\circ$ . Also, physical conditions existing in the region of emitting spots may alter photon emission as in the case of some radio pulsars. Accordingly, we consider the effects of including cosine and sine beaming functions in the calculations of the waveforms.

Figure 2 shows the waveforms from a single emitting spot (left-hand column) and two emitting spots (right-hand column) for various spot sizes. As expected, the amplitude of the intensity oscillations decreases as the spot size increases. Furthermore, in the case of a single emitting spot there is a critical spot size ( $\alpha \sim 50^\circ$  for the case of  $R/M = 5.0$ ) at which the spot is never completely out of view and hence the intensity remains greater than zero for the entire rotational phase. As the waveforms illustrate, the cosine beaming function, which enhances emission along the magnetic field axis, tends to narrow the width of the waveform peaks. The sine beaming function enhances emission near the tangential plane and will produce a four peaked waveform for the case of a small single emitting spot (see Pechenick et al. 1983).

### 3.2. Effects of Spot Size and Light Deflection

We are also interested in the effect of the compactness of the star on the observed amplitudes. Figure 3a shows the fractional rms amplitudes at the first two harmonics as a function of spot size and stellar compactness for one emitting spot centered at  $\beta = \gamma = 90^\circ$  (i.e., for an observer and spot both in the rotational equator). The curves for the first harmonic illustrates the general shape of most of the first harmonic curves. Initially, the amplitude depends only weakly on spot size. However, once the spot grows to  $\sim 40^\circ$  there is a steep decline in the oscillation amplitude which

flattens out only near the tail of the expansion. Figure 3b shows the fractional rms amplitude at the second harmonic under the same assumptions but for two identical, antipodal emitting spots. The range in spot size here is  $0^\circ - 90^\circ$  since two antipodal spots of  $90^\circ$  radii cover the entire stellar surface. Note that in this situation, there is no first harmonic.

These curves illustrate two interesting features of the two spot configuration. First, the strength of the strongest oscillation amplitude in the two spot case is  $\sim 90\%$  weaker than the strength of the strongest oscillation amplitude in the one spot case considered above. Furthermore, the curve of the second harmonic does not exhibit the same sharp falloff seen in the first harmonic curve. Thus, the detection of a particularly large fractional rms amplitude with a steep amplitude decline can verify that what is being observed is a first harmonic (i.e., power generated at the stellar spin frequency) rather than any higher harmonics (see Miller & Lamb 1998). The second interesting feature is that the curve of the second harmonic in Figure 3b is nearly identical in both magnitude and shape to the first  $90^\circ$  of the curve of the second harmonic for the case of one spot shown in Figure 3a. Thus, for this geometry, the introduction of a second emitting spot antipodal to the first tends to destroy the first harmonic while leaving the second harmonic unaffected. This result obtains whenever: (1) the physical assumptions (e.g., compactness, rotational velocity, flux distribution function) made for both the one and two spot configurations are the same, and (2) the viewing geometry for both configurations is  $\beta = \gamma = 90^\circ$ .

In this figure we also display the effect gravity has on the oscillation amplitudes. From equation (3) we know that more compact stars have a larger  $\phi_{max}$ , and hence a larger fraction of their surface is visible to observers. As a result, oscillation amplitudes for more compact neutron stars are smaller. An exception occurs at the second harmonic of very compact stars ( $R/M < 4.0$ ), in which case gravitational light deflection focuses the emitted radiation enough to raise the oscillation amplitude (see Pechenick et al. 1983 and Miller & Lamb 1998). Note that the stellar compactness affects the amplitude at the second harmonic far more than the amplitude at the first harmonic.

### 3.3. Effects of Viewing Angle and Magnetic Inclination

Figure 4a shows the oscillation amplitude as a function of  $\beta = \gamma = x$  (i.e., for the observer and the center of the spot at the same rotational latitude) for a single emitting spot with  $\alpha = 15^\circ$  and  $R/M = 5.0$ . As  $x$  increases, the width of the peaks in the light curve decrease (see Pechenick et al. 1983) and hence the oscillation amplitudes increase. The interesting feature here is that the second harmonic has a significant amplitude only for  $x > 60^\circ$ . Since 50% of the time  $x$  will be between  $60^\circ$  and  $90^\circ$  (assuming randomly distributed observers), only half of all observers will detect a second harmonic during a typical burst involving one spot. In Figure 4b we make the same assumptions as in Figure 4a but for two emitting spots rather than one. If we had assumed flat space-time and an infinitesimal spot size then the second emitting spot would become visible only for  $2x = 180^\circ - \phi_{max} = 180^\circ - 90^\circ = 90^\circ$ . Therefore, for  $x < 45^\circ$  only one spot would be

observable. For  $R/M = 5.0$ ,  $\phi_{max} = 128^\circ$ , and therefore a second, infinitesimal, spot would begin to be visible at  $x = 26^\circ$ . Since in Figure 4, the calculation was done with  $\alpha = 15^\circ$ , the spot begins to become visible at  $x = 26^\circ - (15/2)^\circ \approx 20^\circ$ , explaining the appearance of the second harmonic at this  $x$  value. Note that in the two spot case the first harmonic generates significant power for a wide range of  $x$ . This occurs because for  $x \neq 90^\circ$  one spot is more directly aligned with the observer’s line of sight, and as a result the intensity maxima of the two spots are unequal. In general, whenever an asymmetry exists between the two emitting spots such that the intensity maxima of the two spots are unequal, power is generated at the first harmonic.

### 3.4. Effects of Anisotropies from Doppler Shifts and Beaming

In Figure 5 we include the effects of Doppler shifts and aberrations on the oscillation amplitudes. We assume a surface rotation velocity of  $v = 0.1c$ , which corresponds to a neutron star with radius  $R = 10$  km and spin frequency  $\nu \approx 400$  Hz. As can be seen, the amplitude of the second harmonic is increased significantly more than the amplitude of the first harmonic as a result of rotation. The tendency to generate more power at the higher harmonics than at the spin frequency is a general property of the rotation (see Miller & Lamb 1998 for a discussion of this effect).

Physical conditions in the region of emitting spots might cause anisotropic emission of radiation. The results of including a cosine beaming function and a sine beaming function for the case of one spot are shown in Figure 6a and for two antipodal spots in Figure 6b. As is apparent from Figure 2, the enhanced emission along the magnetic axis for the cosine beaming tends to narrow peaks in the light curves (see Pechenick et al. 1983 for a discussion of the light curves for beamed emission) and hence raise the oscillation amplitudes. For the sine beaming the peaks in the light curve are broadened, tending to lower the amplitude at the first harmonic. Both beaming functions do, however, generate substantial additional power at the higher harmonics.

## 4. APPLICATION TO X-RAY BURST SOURCES

### 4.1. Relative Amplitudes of Harmonics in 4U 1636–536

Recent work by Miller (1999) gives evidence for the presence of power at the stellar spin frequency for a source (4U 1636–536) consisting of two emitting spots. Earlier we saw that one possible mechanism for generating significant power at the stellar spin frequency for the case of two emitting spots is to vary the viewing geometry. Another possible mechanism is to have the spots be non-antipodal. This can occur, for instance, if the star’s dipolar magnetic field has its axis slightly displaced from its center. In the left panel of Figure 7 we show the oscillation amplitude as a function of spot separation for the case of two emitting spots with  $\alpha = 30^\circ$ ,  $\beta = \gamma = 90^\circ$ ,

and  $R/M = 5.0$ . The spots are perfectly antipodal at a spot separation of  $180^\circ$ . As the figure shows, the oscillation amplitude at the second harmonic is relatively constant while the oscillation amplitude at the first harmonic is a linear function of spot separation. At a spot separation of  $\sim 170^\circ$  the fractional rms amplitudes of the first and second harmonic are equal. Another way to produce power at the spin frequency is to have differences in brightness between the two spots. Such an asymmetry can occur, for example, if the strength of the magnetic field at the location of the two spots is different, thereby pooling different amounts of nuclear fuel onto the hot spot regions. In the right panel of Figure 7 we show the oscillation amplitude as a function of the percent difference between the brightness of the two spots. As in the case of the non-antipodal spots, the amplitude at the second harmonic is essentially constant while the amplitude at the first harmonic increases linearly with increasing percent difference in spot brightness.

These figures reinforce the conclusion, also evident from Figure 3, that only with two spots can the oscillation at the first overtone be stronger than the oscillation at the fundamental. Therefore, within the general theoretical model explored in this paper, 4U 1636–536 has two nearly antipodal hot spots.

#### 4.2. Phase Lags in SAX J1808–3658

*Doppler model of phase lags.*—The hard X-ray spectrum of low-mass X-ray binaries is well-fit by a Comptonization model, in which the central neutron star is surrounded by a hot corona of electrons and the photons injected into this corona are relatively soft. It was therefore expected that the observed hard photons, having scattered more often than the soft photons and thus having a longer path length before escape, would lag the soft photons. Instead, in several sources a hard *lead* was discovered. One explanation for this lead was suggested by Ford (1999). He proposed that Doppler shifting of photons emitted from rotating hot spots, as in thermonuclear burst oscillations, would tend to produce a hard lead because the approaching edge of the spot would precede the trailing edge. He compared a simplified calculation of this effect with burst data for Aql X-1 and showed that an adequate fit could be obtained (Ford 1999).

The millisecond X-ray pulsar SAX J1808–3658 provides a stronger test of this hypothesis. This source has strong oscillations ( $\sim 5\%$  rms) at  $\sim 401$  Hz, which as usual are attributed to rotational modulation of a hot spot on the surface. Cui, Morgan, & Titarchuk (1998) obtained precise measurements of the oscillation phase as a function of energy, and found that in this source as well there is a hard lead.

Figure 8 shows sample calculations of the time lag as a function of energy. In the left panel we focus on the dependence of the lag on mass, and in the right panel we concentrate on the effect of changing the surface temperature. In both cases the surface emission pattern is the pattern for a gray atmosphere, and we assume  $R/M = 5.1$  and a stellar spin frequency of 401 Hz, which is the spin frequency of SAX J1808–3658. In panel (a) we assume a surface effective temperature

of  $kT = 0.7$  keV as measured at infinity. In panel (b) we assume a stellar gravitational mass of  $1.6 M_{\odot}$ , which gives a surface equatorial rotation velocity of  $0.1 c$  as measured at infinity. From this figure it is clear that the effect of increasing the mass is to increase the phase lead, whereas the effect of increasing the temperature is to increase the energy at which the curve starts to flatten.

*Comparison with data.*—Comparing these models with the data for SAX J1808–3658 introduces additional complications. In order to improve statistics, Cui et al. (1998) averaged the phase lags over the period from 11 April 1998 to 29 April 1998. The calculation of the phase leads by Cui et al. (1998) also involves averaging the phase over energy bins several keV in width. Examination of Figure 9 shows that the phase changes rapidly over such an energy range, implying that the measured phase lead depends sensitively on the input spectrum. The effective area of RXTE also decreases rapidly below 4 keV, which strongly affects the observed average phase in the 2–3 keV reference bin. Finally, given that the observed spectrum is not a blackbody, but is instead approximately a power law of index 1.86 from  $\sim 3$  keV to  $\sim 30$  keV (Heindl & Smith 1998), Compton reprocessing has taken place and the observed phase lags are the result of a convolution between the unscattered phase lags and the Compton redistribution function.

Figure 9 plots the data along with a simplified model of the phase lags taking some of these complications into account. We ignore the changing effective area of RXTE and assume a constant response with energy. Based on the power-law nature of the spectrum, we approximate the process of Comptonization by assuming that the energy of the injected photons is much less than the observed photon energies or the temperature of the electrons. We also assume an isothermal atmosphere, in contrast to the gray atmosphere we used for Figure 8, which gives too low a hard lead. The best fit has  $kT = 1.1$  keV as observed at infinity,  $R = 10$  km, and  $M = 2.2 M_{\odot}$ . The total  $\chi^2$  of the fit is 38.6 for 6 degrees of freedom. The dominant contribution to this  $\chi^2$  comes from the underprediction of the hard lead at low energies. This is as expected, because we assumed an instrumental effective area that is constant with energy, whereas in reality the effective area rises rapidly with increasing photon energy at low energies. This changing effective area gives greater weight to the larger leads at higher energies, which is in better agreement with the data. Therefore, given the simplifications of the model, our fit to the data is encouragingly good and supports the Doppler interpretation of the observed hard lead.

## 5. DISCUSSION

*Relative amplitudes of harmonics.*—We have presented calculations of the waveforms and amplitudes at different harmonics of the spin frequency for one or two hot spots and many realistic combinations of stellar compactness, spot size and emission pattern, observation angle, and magnetic inclination. These calculations show that typically either the fundamental or the first overtone has an amplitude much larger than the amplitude of any other harmonic. This corresponds well to the observations of the six sources with burst brightness oscillations, in which there is a strong oscillation at only one frequency. We also find that if the first overtone is the

dominant harmonic, there must be two similar and nearly antipodal bright spots, because a single spot always produces a much stronger oscillation at the fundamental than at any overtone. In contrast, if the fundamental is much stronger than the overtone, this is consistent with but does not require a single spot: if there are two bright spots that are sufficiently dissimilar or far away from antipodal, or if our line of sight is such that one of the spots is hidden, then the oscillation at the fundamental will dominate. This implies that the three sources with detectable oscillations near  $\sim 300$  Hz (4U 1728–34 [Strohmayer et al. 1996], 4U 1702–43 [Markwardt, Strohmayer, & Swank 1999], and 4U 1636–536 [Miller 1999; this source has a strong oscillation at  $\sim 580$  Hz but a detectable oscillation at  $\sim 290$  Hz]) have spin frequencies of  $\sim 300$  Hz, whereas the three sources with detectable oscillations only at  $\sim 500$ – $600$  Hz (Aql X-1 [Zhang et al. 1998], MXB 1743–29 [Strohmayer et al. 1997a], and KS 1731–260 [Smith et al. 1997]) could have spin frequencies at either this frequency or half of it. Therefore, all six burst oscillation sources are consistent with having spin frequencies  $\sim 300$  Hz.

*Information content of waveforms.*—Our results also show clearly that power density spectra, which contain information only on the relative amplitudes of different harmonics, are much less informative than the waveforms themselves. Figure 10 shows three different waveforms that all have an amplitude at the first overtone that is 2.3 times the amplitude at the fundamental, which is the ratio found by Miller (1999) for 4U 1636–536. In all three cases there are two bright spots. The solid line shows the waveform for two identical pointlike spots that are  $175^\circ$  apart, the dotted line shows the waveform for two antipodal spots with brightnesses differing by 10%, and the dashed line shows the waveform for two identical and antipodal spots that are  $75^\circ$  from the rotational pole and observed from a line of sight that is also  $75^\circ$  from the rotational pole. Although the amplitude ratio is the same in each case, the waveforms are quite different from each other, and the physical implications are also different. This underscores the importance of calculating waveforms and not just power density spectra, both observationally and theoretically.

*Searches for weak higher harmonics.*—The amplitudes and phases of higher harmonics potentially contain important clues about the propagation of nuclear burning and about the compactness of the star, but as yet there are no sources in which a higher harmonic of a strong oscillation has been observed. Our plots of amplitude versus spot size suggest that it is best to look for weaker higher harmonics when the dominant oscillation is strong. The reason is that, in general, the ratio of the second to first harmonic drops with increasing spot size, and therefore with decreasing amplitude at the fundamental. Hence, a search only of data showing strong oscillations may more sensitively reveal the presence of higher harmonics.

*Shape of amplitude decrease as a function of spot size.*—In our calculations, as the spot size increases the amplitude decreases slowly until the angular radius of the spot is  $\sim 40^\circ$  but quickly thereafter. This apparently conflicts with the observations of 4U 1728–34 reported in Strohmayer et al. (1997), in which the error bars are large but it appears that the decrease in amplitude is fast from the start and then slows down. Further quantification of this result is important, but if confirmed it could be caused by a number of effects. For example, the spot size might never

be small: if ignition were nearly simultaneous over a large area, further spreading would already be in the large-spot regime, and hence the amplitude would decrease quickly. If the spreading velocity were initially high but then decreased, this would have a similar effect on the amplitudes. Alternately, if there is a corona with a non-negligible scattering optical depth around the star and the optical depth increases as the burst approaches its peak flux, this would also decrease the amplitude faster than expected when the optical depth is zero.

*Phase lags as a probe of surface rotation velocity.*—We find that the hard lead observed in SAX J1808–3658 is fit reasonably well by a model (see Ford 1999) in which rotational Doppler shifts cause higher-energy X-rays to lead lower-energy X-rays. This fit lends support to the model, and suggests that with better fitting and more data (especially from a future high-area timing mission) it may be possible to use phase lag versus energy data to help constraint the mass  $M$  or the compactness  $R/M$  of the star.

We thank Wei Cui for providing time lag data for SAX J1808-3658. This work was supported in part by NASA ATP grant number NRA-98-03-ATP-028, NASA contract NASW-4690, and DOE contract DOE B341495.

## REFERENCES

- Bildsten, L. 1995, ApJ, 438, 852  
Cui, W., Morgan, E. H., & Titarchuk, L. G. 1998, ApJ, 504, L27  
Ford, E. C. 1999, ApJ, 519, L73  
Fryxell, B. A., & Woosley, S. E. 1982, ApJ, 258, 733  
Heindl, W. A., & Smith, D. M. 1998, ApJ, 506, L35  
Lamb, F. K., & Miller, M. C. 1995, ApJ, 439, 828  
Markwardt, C. B., Strohmayer, T. E., & Swank, J. H. 1999, ApJ, 512, L125  
Miller, M. C., 1999, ApJ, 515, L77  
Miller, M. C., & Lamb, F. K. 1996, ApJ, 470, 1033  
Miller, M. C., & Lamb, F. K. 1998, ApJ, 499, L37  
Misner, C.W., Thorne, K.S., and Wheeler, J.A. 1973, *Gravitation* (San Francisco; Freeman)  
Nozakura, T., Ikeuchi, S., & Fujimoto, M. Y. 1984, ApJ, 286, 221  
Pechenick, K. R., Ftaclas, C., & Cohen, J. M. 1983, ApJ, 274, 846  
Smith, D., Morgan, E. H. & Bradt, H. V. 1997, ApJ, 479, L137  
Strohmayer, T. E., 1992, ApJ, 388, 138  
Strohmayer, T. E., Jahoda, K., Giles, A. B., & Lee, U. 1997a, ApJ, 486, 355

Strohmayer, T. E., Zhang, W. & Swank, J. H. 1997b, ApJ, 487, L77

Strohmayer, T. E., Zhang, W., Swank, J. H., Smale, A. P., Titarchuk, L., & Day, C. 1996, ApJ, 469, L9

Strohmayer, T. E., Jahoda, K., Giles, A. B. & Lee, U. 1997c, ApJ, 486, 355

Zhang, W., Lapidus, I., Swank, J. H., White, N. E. & Titarchuk, L. 1996, IAUC 6541

Zhang, W., Jahoda, K., Kelley, R. L., Strohmayer, T. E., Swank, J. H., Zhang, S. N. 1998, ApJ, 495, L9

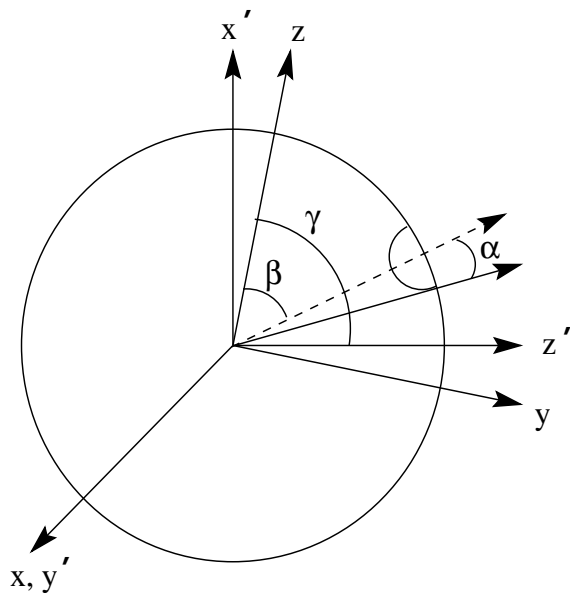


Fig. 1.— Coordinate systems used in this paper. The unprimed axes correspond to a frame fixed with respect to the star, in which the  $z$ -axis is the stellar rotation axis. The hot spot is fixed on the star and rotates with it; the center of the hot spot is an angle  $\beta$  from the rotation axis, and the angular radius of the hot spot is  $\alpha$ . The primed axes are for a coordinate system at rest with respect to the observer at infinity, who is in the direction corresponding to the positive  $z'$  axis, at an angle  $\gamma$  from the rotation axis. This figure is based on a similar figure in Strohmayer (1992).

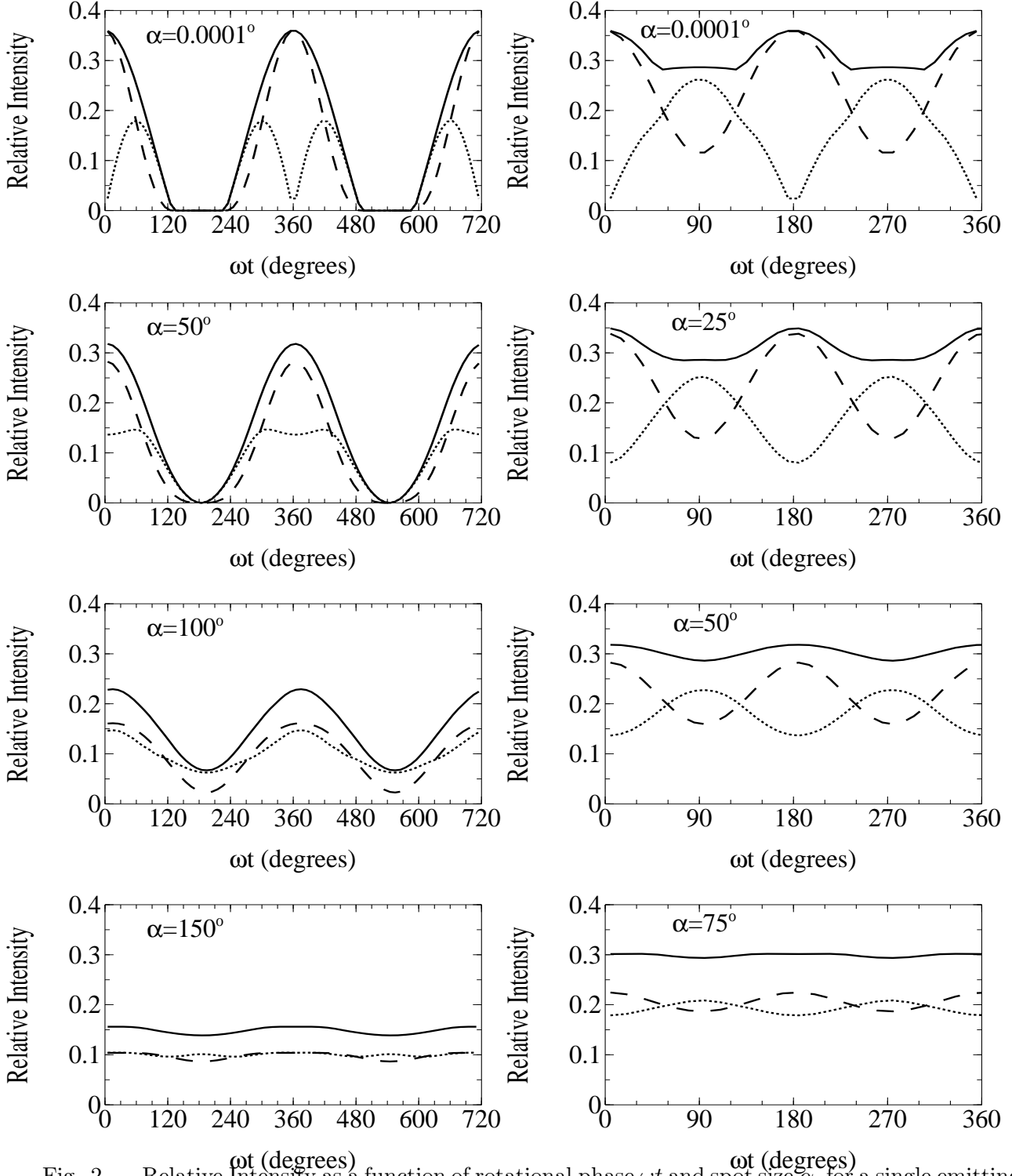


Fig. 2.— Relative Intensity as a function of rotational phase  $\omega t$  and spot size  $\alpha$ , for a single emitting spot (left column) and two emitting spots (right column) with  $R/M = 5.0$  and  $\beta = \gamma = 90^\circ$ . Solid line is isotropic emission, dashed line is cosine beaming and dotted line is sine beaming. As the spot sizes increase the amplitude of the intensity oscillations decrease. Cosine beaming narrows the width of the waveform peaks and sine beaming produces four peaked waveforms for small single emitting spots.

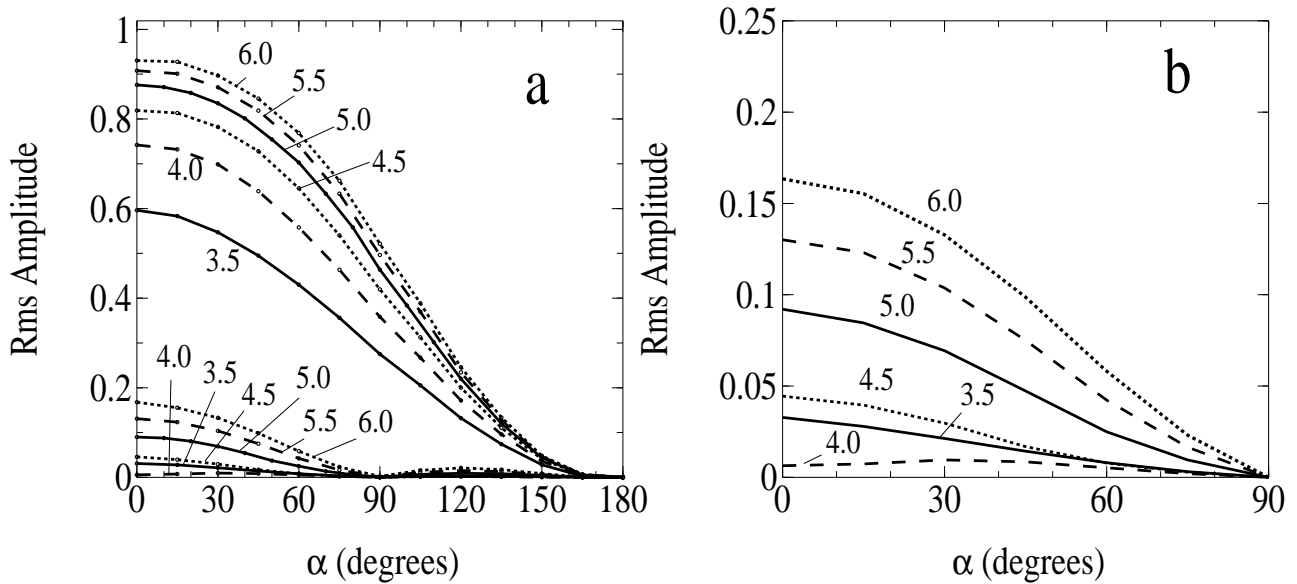


Fig. 3.— (a) Rms amplitude as a function of spot size  $\alpha$  and stellar compactness at the first harmonic (upper curves) and the second harmonic (lower curves) from a single emitting spot. Numbers denote the value of  $R/M$  used for each curve (where we use geometrized units in which  $G = c \equiv 1$ ), and in each case we assume  $\beta = \gamma = 90^\circ$ , i.e., that both the observer and the center of the spot are in the rotational equator. (b) Rms amplitude as a function of spot size and stellar compactness at the second harmonic from two antipodal emitting spots. Note that the vertical scale is different than in panel (a). As before, numbers denote  $R/M$  and we assume  $\beta = \gamma = 90^\circ$ . These figures show that the amplitude remains relatively unchanged as the spot size increases until  $\alpha \sim 40^\circ$ , at which point the amplitude drops sharply. It is therefore expected that, if thermonuclear propagation proceeds at a constant and slow speed, the amplitude versus time curve should initially exhibit negative curvature. These figures also show that the bolometric amplitude at the second harmonic is much more strongly affected by the stellar compactness than is the amplitude at the first harmonic.

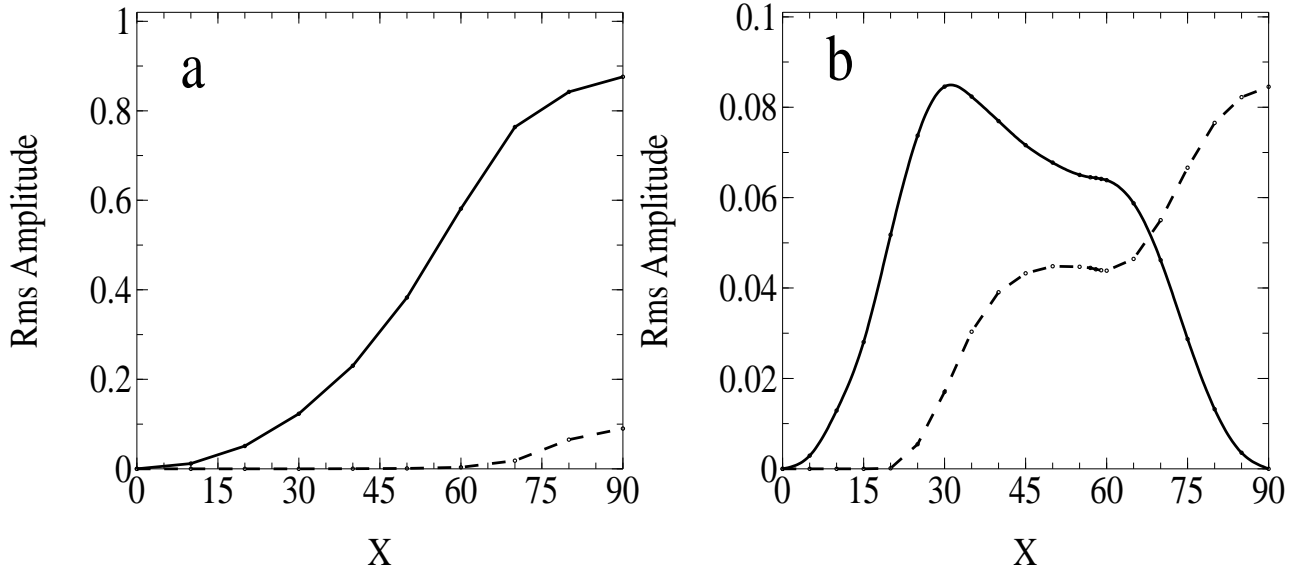


Fig. 4.— Rms amplitude as a function of  $\beta = \gamma = X$  (i.e., for an observer at the same angular distance from the rotation as the hot spot is). (a) Single emitting spot with  $R/M = 5.0$  and  $\alpha = 15^\circ$ . The solid line plots the amplitude of the first harmonic, and the dashed line plots the amplitude of the second harmonic. This panel demonstrates that if there is only one spot, the presence of a second harmonic means that the line of sight of the observer cannot be close to face-on. (b) Two antipodal emitting spots, where again  $R/M = 5.0$  and  $\alpha = 15^\circ$ , and the amplitudes of both the first harmonic (solid line) and second harmonic (dashed line) are plotted. This panel shows that as the line of sight and location of the hot spot move from the rotational axis to the rotational equator, the power in the first harmonic is gradually transferred to the second harmonic.

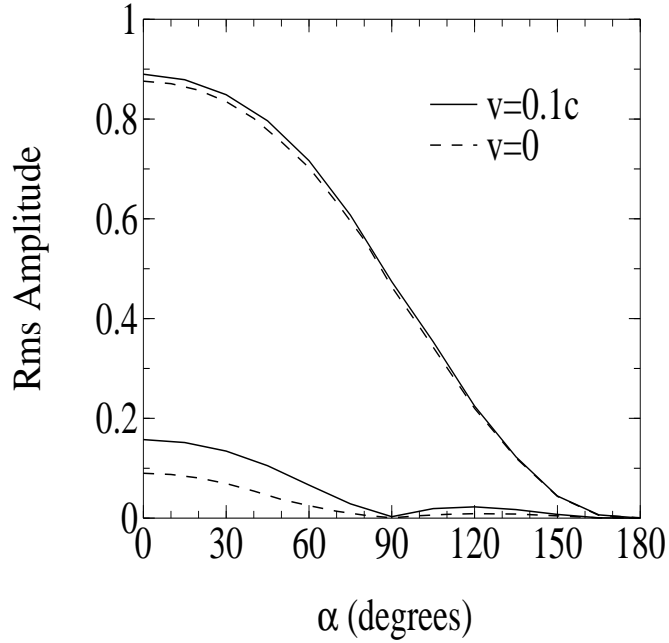


Fig. 5.— Effect of surface rotational velocities on different harmonics. Here we plot rms amplitude vs. spot angular radius  $\alpha$  at the first harmonic (upper curves) and the second harmonic (lower curves) from a single emitting spot with a surface velocity measured at infinity of  $v = 0.1c$  (*solid lines*) and  $v = 0.0c$  (*dashed lines*),  $R/M = 5.0$ , and  $\beta = \gamma = 90^\circ$  (i.e., observer and hot spot both in the rotational equator). The increase in amplitude due to nonzero rotational velocities is much greater for overtones than it is for the fundamental of the stellar spin frequency.

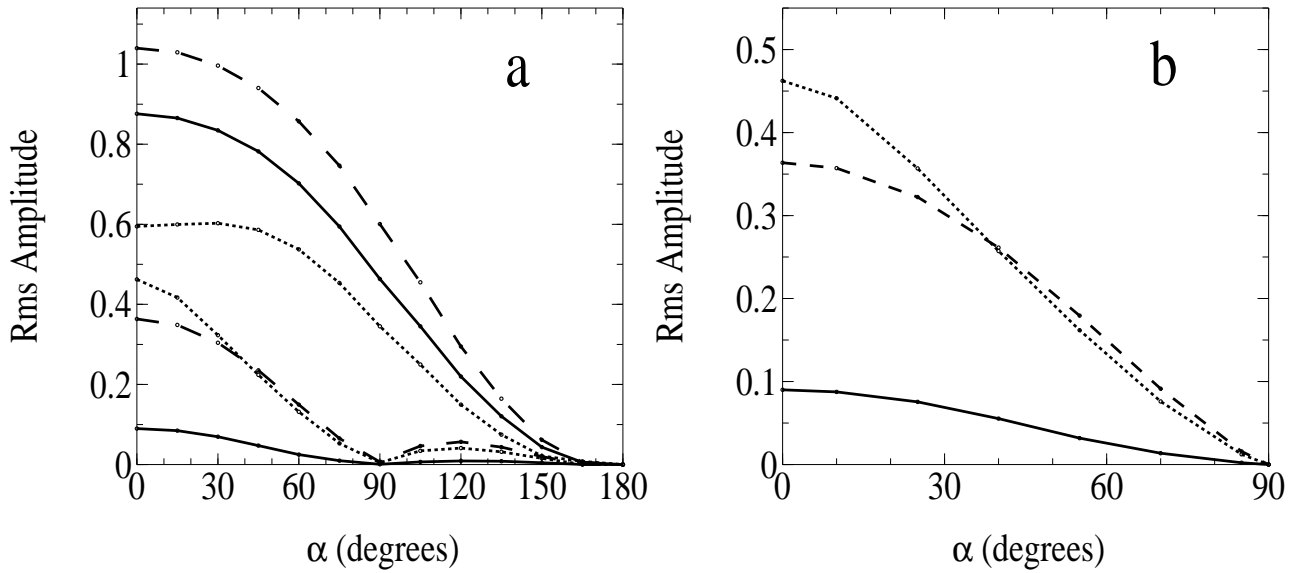


Fig. 6.— Effect of different beaming functions on the first and second harmonics. (a) Rms amplitude vs.  $\alpha$  at the first harmonic (upper three curves) and the second harmonic (lower three curves) from a single emitting spot with  $R/M = 5.0$ ,  $\beta = \gamma = 90^\circ$ . Dashed line is cosine beaming, solid line is isotropic emission, and dotted line is sine beaming. (b) Rms amplitude vs.  $\alpha$  at the second harmonic from two emitting spots with  $R/M = 5.0$ ,  $\beta = \gamma = 90^\circ$ . Again, dashed line is cosine beaming, solid line is isotropic emission, and dotted line is sine beaming. Both of the anisotropic emission patterns enhance tremendously the amplitude at the second harmonic, by a factor of at least 4.

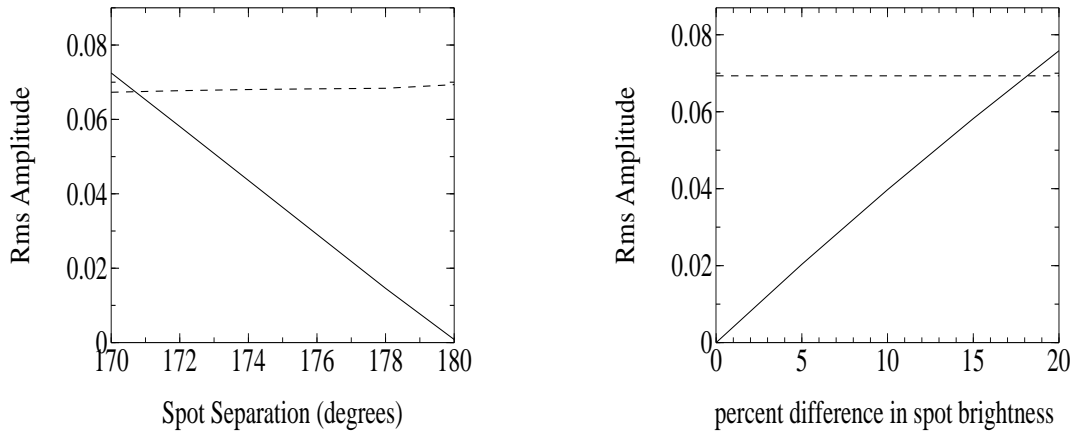


Fig. 7.— Effect of nonantipodal separation of spots and differences in spot brightness on the relative amplitudes at the first and second harmonics. (left panel) Rms amplitude vs. spot separation at the first harmonic (*solid line*) and the second harmonic (*dashed line*) for two emitting spots with  $R/M = 5.0$ ,  $\alpha = 30^\circ$ ,  $\beta = \gamma = 90^\circ$ . (right panel) Rms amplitude vs. percent difference in spot brightness at the first harmonic (*solid line*) and the second harmonic (*dashed line*) for two antipodal emitting spots with  $R/M = 5.0$ ,  $\alpha = 30^\circ$ ,  $\beta = \gamma = 90^\circ$ . The analysis of RXTE data from 4U 1636–536 by Miller (1999) indicates that the average ratio of amplitudes of the second to first harmonic is 2.3. This figure therefore places strong constraints on the spot separation and possible differences in spot brightness: the spot separation in 4U 1636–536 must be within  $4^\circ$  of antipodal, and the spot brightnesses must be within 7% of each other, or else the amplitude at the fundamental of the spin frequency would be larger than observed relative to the overtone.

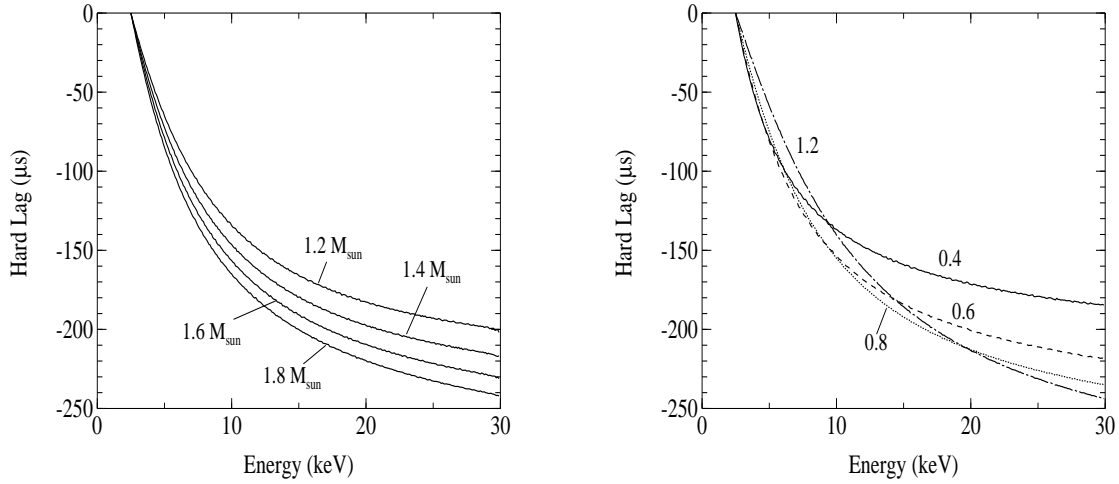


Fig. 8.— Time lags versus photon energy, as a function of stellar gravitational mass (left panel) and of surface temperature (right panel). The lags are relative to the photons at 2.5 keV, and their negative value indicates a hard lead. In both cases we assume a stellar spin frequency of 401 Hz to correspond to the spin frequency of SAX J1808–3658. We also assume a stellar compactness of  $R/M = 5.1$ , and assume that the surface emission has the pattern appropriate for a gray atmosphere. In the left panel the curves are labeled by the gravitational mass, and we assume a surface effective temperature of  $kT = 0.7$  keV as measured at infinity. In the right panel the curves are labeled by the surface effective temperature (as measured at infinity) in units of keV, and we assume  $M = 1.6 M_{\odot}$ .

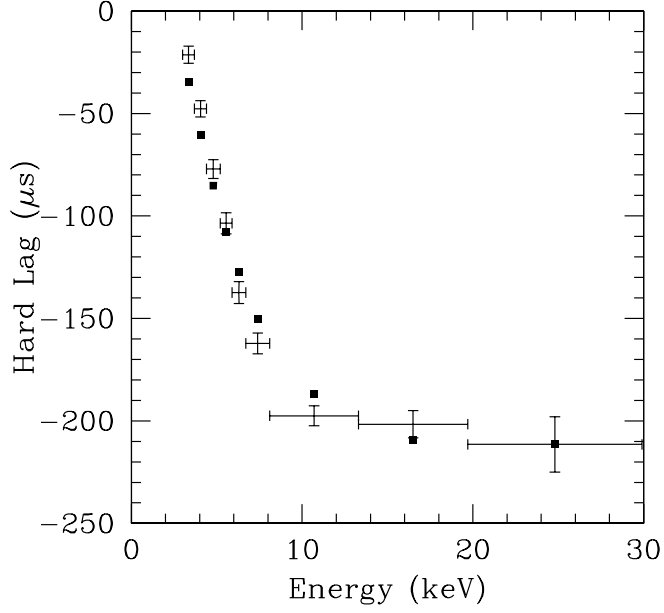


Fig. 9.— Comparison of model time lags with the lags reported by Cui et al. (1998) for SAX J1808–3658. The vertical axis is the time lag in microseconds relative to the average in the 2–3 keV band, and the horizontal axis is the observed photon energy in keV. The crosses are the data: the horizontal bars indicate the extent of each energy bin, whereas the vertical bars indicate the uncertainty in the time lag. The model time lags are shown with the filled boxes, and are computed via the procedure described in the text. In this fit, the neutron star gravitational mass is  $M = 2.2 M_{\odot}$ ,  $R = 10$  km, the surface temperature measured at infinity is  $kT = 1.1$  keV, and we assumed an isothermal atmosphere. The total  $\chi^2$  was 38.6 for six degrees of freedom. The reasonable quantitative fit to the data add support to the Doppler shift hypothesis for the origin of the hard leads. The data for SAX J1808–3658 were kindly provided by Wei Cui.

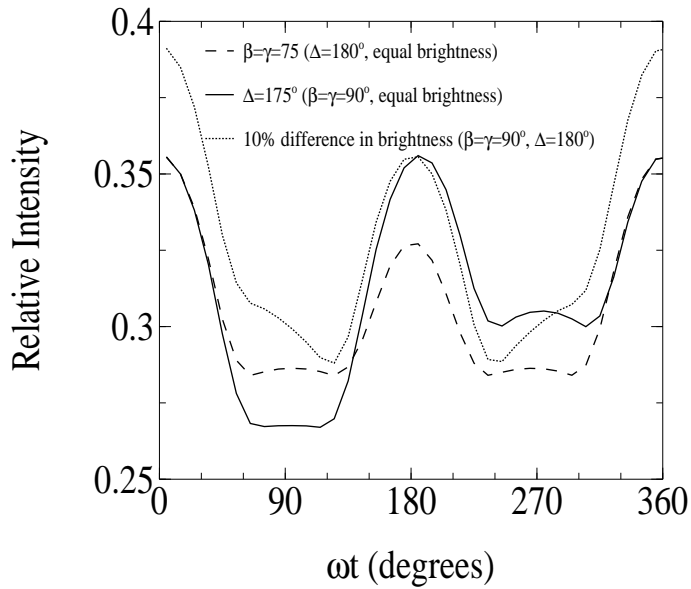


Fig. 10.— Burst oscillation waveforms with a fixed ratio between the amplitude at the first overtone and the amplitude at the fundamental of 2.3, which was the ratio found by Miller (1999) for 4U 1636–536. Solid line: identical spots  $175^\circ$  apart. Dotted line: antipodal spots differing in brightness by 10%. Dashed line: identical, antipodal spots  $75^\circ$  from the rotation axis as seen by a distant observer  $75^\circ$  from the rotation axis. For all three curves,  $R/M = 5$  and the spot angular radius is  $15^\circ$ . This figure shows that amplitude ratios, as are computed with a power density spectrum, are not sufficient to distinguish between these various scenarios. Waveforms are to be preferred.